Sirius: A Self-Localization System for Resource-Constrained IoT Sensors

Nakul Garg, Nirupam Roy
University of Maryland, College Park
{nakul22, niruroy}@umd.edu

ABSTRACT

Low-power sensor networks are transforming large-scale sensing in precision farming, livestock tracking, climate-monitoring and surveying. Accurate and robust localization in such low-power sensor nodes has never been as crucial as it is today. This paper presents, *Sirius*, a self-localization system using a single receiver for low-power IoT nodes. Traditionally, systems have relied on antenna arrays and tight synchronization to estimate angle-of-arrival (AoA) and time-of-flight with known access points. While these techniques work well for regular mobile systems, low-power IoT nodes lack the resources to support these complex systems. *Sirius* explores the use of gain-pattern reconfigurable antennas with passive envelope detector-based radios to perform AoA estimation without requiring any kind of synchronization. It shows a technique to embed *direction specific codes* to the received signals which are transparent to regular communication channel but carry AoA information with them. *Sirius* embeds these direction-specific codes by using reconfigurable antennas and fluctuating the gain pattern of the antenna. Our prototype demonstrates a median error of 7 degrees in AoA estimation and 2.5 meters in localization, which is similar to state-of-the-art antenna array-based systems. *Sirius* opens up new possibilities for low-power IoT nodes.

CCS CONCEPTS

• **Computer systems organization** → **Sensor networks**; **Embedded systems**; **Sensors and actuators**.

KEYWORDS

Low-power sensing; IoT; Ultra-low-power localization; Embedded AI; Low-power antenna

1 INTRODUCTION

Advancements in miniaturized, ultra-low-power localization techniques have enabled new opportunities in long-term monitoring and behavior studies of wildlife and livestocks over

Traditional antenna array approach:
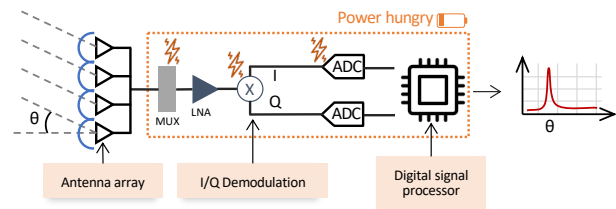
***Sirius*:**

Figure 1: *Sirius* dynamically switches the beam pattern of the antenna to embed direction specific signature to the received signal. The vector of amplitudes contain the unique signature which map to the angle-of-arrival, θ.

a large open field. Sensor nodes a few centimeters in size and a few grams in weight have shown capability to self-localize and save data for several days and intermittently radio out the data to the nearby gateways. Communication b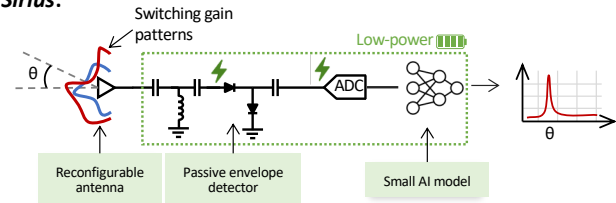eing one of the core component of this model, existing solutions often compromise on the location accuracy in order to fit communication and sensing functionalities within available power budget. In this paper, we present *Sirius*, which breaks this trade-off by using a single antenna and radio to simultaneously communicate and self-localize within millijoules of power requirement and millimeters in size.

Self-localization, where the node computes its location onboard, is particularly challenging on small and low-power nodes. Conventional sensors for location estimation are power hungry. GPS uses low-noise amplifiers requiring several milliWatts of power to receive weak satellite signals (-155 dBm) for location fixes [63]. Power requirement of Ultra-wideband (UWB) radio or Bluetooth-Low-Energy (BLE) based solutions can go up to a half of a Watt along with synchronization and other protocol overhead [37]. Fundamentally localization relies on two different spatial features extracted from the received signal – the distance from the source and the angle-of-arrival (AoA). A node can use a combination of distances and/or AoAs from multiple sources to estimate its location with respect to the known locations of the sources [16, 17, 68]. Distance estimation requires strict time synchronization [68] between the node and the source so that

time-of-flight (ToF) of the signal can be measured accurately. Given the signal travels at the speed of the light, a small error in synchronization can lead to several meters of error in distance and, in turn the location estimate. Onboard clock of the low-cost nodes are prone to drift and require frequent coordination with the access point, which is not a desired behavior for ultra-low-power nodes [1]. Moreover, the time resolution of the ToF estimate is inversely proportional to the radio-bandwidth. The low-bandwidth communication radios can not meet the requirement.

AoA-based localization methods, on the other hand, do not require strict coordination with the access points and are more suitable for independent self-localization on the low-power nodes [17, 58]. Triangulation using AoAs from two unsophisticated beacons can be sufficient for the node to find its position. However, existing methods require complex hardware for AoA estimation. Spatial sampling to find the angle of arrival of the signal requires an array of antennas separated by at least half-wavelength distance. [38, 72] Antenna arrays lead to power-hungry radio frontend and a bigger space for low-frequency antenna. Spatial scanning using steerable beams – computational or mechanical – consumes several times the available power per duty cycle in these nodes. We propose an efficient method that uses angles and does not require phase information. *Sirius*'s single antenna based design reduces the form factor and power consumption of the node.

Communication and localization are often designed to work on the same radio. Passive envelope detector-based radio architectures are evolving in low-power nodes. Several recent works [15, 40, 57, 75] focused on improvements in this communication architecture to achieve reliable data exchange at a ultra-low power budget. However, few attempts have been made on solving localization using envelope detector based architecture. This is mainly due to the reason that envelope detectors eliminate power hungry components of radio such as oscillators and high speed ADCs. But due to this, extracting the phase information of UHF waves becomes challenging.

We take a novel approach to obtain the AoA for triangulation we call 'directional code embedding'. The high level idea is to embed a direction specific code to the incoming signal during reception and later post-process the signal to recover the code unique to a specific angle-of-arrival. Imagine a radio receiver capable of fluctuating the amplitude of the signal in a subtle but consistent way that adds a signature to the signal. The fluctuation is designed to remain transparent to regular communication and signal decoding, but the signal processing can identify it as a unique code. Now if we can design this signal fluctuation to be a function of the angle of arrival, the code embedded in the signal will reveal the AoA. We leverage antenna's gain pattern for this purpose. Figure 1 gives an overview of the system.

An antenna is basically a metallic structure that captures and transmits radio electromagnetic waves [61]. Based on the shape of its conductive structure, an antenna can have different gains of reception at different angles. In other words, a simple asymmetric shape of an antenna can amplify or attenuate signals arriving from certain angles to create a unique shape of angular gain pattern.
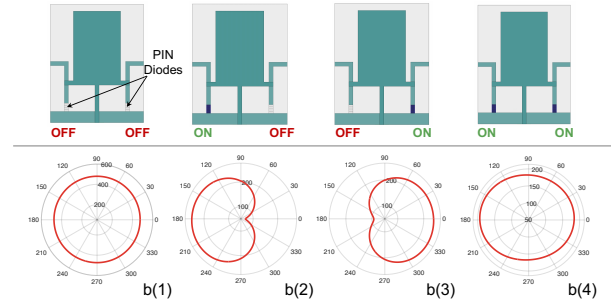

Figure 2: *Sirius* **uses pin-diode to switch the gain pattern of an antenna. Connecting and disconnecting a conductive patch to the surface of antenna can change the shape of the gain pattern. This figure shows four different configurations of the antenna controlled using a set of two switches.**

Typically, this gain pattern is constant as the shape of the conductive structure does not change. However, we have shown that there are multiple independent conductive components on the antenna which are connected through controllable switches. These switches are turned on and off to connect and disconnect a component from the antenna leading to essentially a controllable shape of the antenna. This in turn gives a means to switch between different unique gain patterns in real-time.

Literature is sparse on self-localization methods suitable for envelope detector-based receiver. Probably closest to our work is LivingIoT [33]. It has shown an effective technique to estimate the angles of the access points with respect to the mobile node. Here two or more access points sweep the region with steerable beams in a synchronized pattern so that the mobile node estimates the angle by observing the time of maximum beam power. It requires specialized access points with antenna arrays capable of focusing the beam and also adds a latency on location update while the beam scans the region. *Sirius*, on the other hand, is capable of estimating AoA using only a narrowband signal from the access point or even from a simple beacon. Given the system estimates the AoA from any signal using completely onboard computations, the self-localization requires only two omnidirectional beacons for the reference anchor locations. *Sirius* does not require any synchronization, not even between the anchor beacons. We have developed an ultra-low-power technique to tolerate time-frequency drifts between the transmitters and the receiver. *Sirius* can operate with any low-power envelope-detection based communication architecture while the location estimation process remains transparent to the communication and run in parallel. Table 2 summarizes and highlights the core differences in existing works and *Sirius*.

This paper is a step toward a broader vision of reducing hardware complexity for sensing on the edge devices [6, 18–21]. It strives to relax strict hardware requirements in spatial sensing on these resource-constrained devices by formulating it as primarily a computation and inference problem [6, 17]. This leverages the capabilities of advanced machine intelligence to bridge the limitations of unsophisticated hardware toward achievable performance. Latest microcontrollers make it possible to run these

algorithms on the edge devices without frequent communication with the server to offload processing [7, 17, 32]. This approach not only enables complex sensing on battery-less platforms, but also makes them inexpensive to scale in numbers and it is easier to upgrade the sensing capabilities through software updates. *Sirius* shows a method for signal's angle-of-arrival estimation using a single antenna and an ultra-low-power radio. The core method can be applicable to a number of sensing applications beyond localization. While it opens up scopes for improvements and future research, in this paper we focused on assessing the possibilities and limitations of the system. We have made the following contributions at this stage of the project.

- We present, to the best of our knowledge, the first ultra-low power self-localization system that uses a single antenna and does not require any kind of synchronization.
- We develop a novel angle-of-arrival estimation technique using a single antenna. The technique uses pin-diode based RF switches to switch between multiple beam pattern configurations to capture fine-grained AoA information.
- We develop a novel algorithm to identify anchors and classify its AoA without requiring any time synchronization.
- We implement a functional hardware-software prototype of *Sirius*. We extensively evaluate the prototype on its real world performance and power consumption.

2 CORE INTUITION AND FEASIBILITY

Traditional methods of AoA estimation have relied on spatial sampling or scanning each angle using a directional receiver. A scanning beam is either generated by a highly directional antenna which is mounted on a motor or generated using a phased antenna array. However, both of these approaches are power expensive. Motors consume huge amounts of energy to rotate and are generally limited in motion and speed. On the other hand, antenna arrays fundamentally require spatial sampling of the signal using multiple antennas to extract phase and perform beamforming [38, 71, 72]. This requires power-hungry components such as oscillators, down converters, multiplexers and ADCs which are now becoming obsolete for the future ultra-low-power IOT nodes [40, 66, 67].
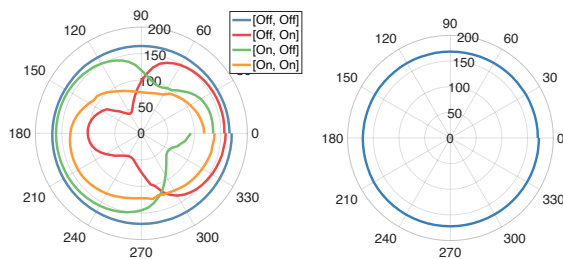

Figure 3: Feasibility study demonstrates dynamic gain pattern switching. Figure shows gain patterns for (a) our reconfigurable antenna and (b) regular antenna.

Our goal with *Sirius* is to enable localization on ultra low-power nodes comprising of passive envelope detectors. The key intuition is to embed a direction specific code using subtle amplitude fluctuations in the received signal, so that even the envelope

detectors can sense these amplitude changes without requiring to sample the phase of the signal.

To embed direction-specific fluctuations, we dynamically change the gain value of the antenna. We design a reconfigurable antenna that can switch between diverse gain patterns on the fly. Figure 1 shows the reconfigurable antenna receiving the signal with multiple gain patterns to create a vector of gain values which uniquely maps to the AoA of the signal.

To reconfigure the gain pattern of an antenna, we change the shape of the antenna. We achieve this by carefully connecting and disconnecting patches of conductor to the antenna using RF switches. To check the feasibility of our idea, we first run a simulation experiment. Figure 2 shows the gain pattern of the simulated antenna where we use pin diodes to connect patches of conductor to either side of the antenna.

We also make a prototype of the designed antenna and perform a simple experiment to verify the switching in the real world. We place a stationary antenna transmitting a pure tone of 900MHz and our reconfigurable antenna a few meters apart mounted on a turntable. We collect the gain pattern of the antenna multiple times while switching between four different antenna configurations. Figure 3 shows the polar plot of the gain pattern of our antenna along with the gain pattern of a regular off-the-shelf omnidirectional antenna. We clearly see the diversity in our antenna which we will use to design our AoA estimation technique.

While the concept looks promising, there are several challenges in designing a practical localization system. Next, we discuss the system challenges in detail.

3 SYSTEM DESIGN

3.1 Ultra-low Power Receiver

In order to minimize the power consumption of *Sirius*, we eliminate the power-consuming parts from the front-end radios like high-frequency oscillators and down converters. We do not sample the amplitude and phase of the signal. Instead, we only sample the energy of the incoming signal using a passive envelope detector. As we discussed in the previous section, we could capture the direction-specific signature by just extracting the energy of the signal. To this end, we use a passive envelope detector to receive the signal which measures the absolute energy of the signal. The output of the envelope detector is rectified voltage which is proportional to the energy of the signal. We capture the voltage using an ultra-low power sigma-delta ADC. The sampling frequency of the ADC is extremely low, in the kHz range, which is orders of magnitude less than the MHz ADCs found in conventional radio receivers. This provides a significant reduction in power as oscillators and ADCs are the most power-hungry components of the radio front-end. Figure 4 shows the circuit diagram of our receiver. *Sirius* does not require any amplifier to increase the SNR of the signal, rather it uses an impedance-matching network to decrease the reflection of the signal from the antenna. We use SMS7630 schottky diodes [59] and microwave grade capacitors and inductors to develop a sensitive and passive front-end for *Sirius*.
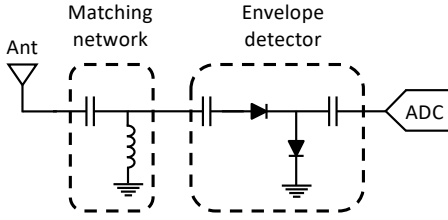
Figure 4: Passive envelope detector used by *Sirius* captures incoming signal energy without requiring power-hungry components such as oscillators and down-converters.

3.2 AoA Estimation

When a signal, $x(t)$, arrives at the antenna surface, the amplitude of the sampled signal, $y(\phi, t)$, is proportional to the gain of the antenna, $G(\phi)$, at a particular angle-of-arrival, ϕ, of the signal.

$$y(\phi, t) = G(\phi)x(t) \tag{1}$$

While most antennas have a fixed gain pattern, we leverage the reconfigurable antenna that can dynamically change its gain pattern using RF switches. We use this antenna to sample the signal with multiple gain patterns, each with its own unique gain value. This gives an array of sampled signals, $[y_1(\phi, t)y_2(\phi, t) \ldots y_n(\phi, t)]$, all with different gain patterns but same angle-of-arrival. Here n is the number of unique gain patterns.

$$\begin{bmatrix} y_1(\phi, t) \\ y_2(\phi, t) \\ \vdots \\ y_n(\phi, t) \end{bmatrix} = \begin{bmatrix} G_1(\phi)x(t) \\ G_2(\phi)x(t) \\ \vdots \\ G_n(\phi)x(t) \end{bmatrix} \tag{2}$$

The amplitudes of this vector, $[|y_1(\phi, t)|, |y_2(\phi, t)| \ldots |y_n(\phi, t)|]$, contains a unique signature about ϕ. However, it is dependent on $|x(t)|$ which can change with transmitting signal strength or the distance between the antennas. We cannot compute AoA, unless we precisely know $|x(t)|$. To solve this, we divide each element of the array with the first element, making the signature independent of the transmitted signal.

$$C = \begin{bmatrix} 1 \\ |y_2(\phi, t)|/|y_1(\phi, t)| \\ \vdots \\ |y_n(\phi, t)|/|y_1(\phi, t)| \end{bmatrix} = \begin{bmatrix} 1 \\ |G_2(\phi)|/|G_1(\phi)| \\ \vdots \\ |G_n(\phi)|/|G_1(\phi)| \end{bmatrix} \tag{3}$$

We extract the signature code induced by the antenna, C, and look it up in a table of pre-learned signatures that corresponds to the AoA, ϕ.

Effects of multipath: Our formulation for AoA estimation assumes that the gain pattern of the antenna can be used for decoding. However, the presence of reflecting surfaces in the environment can affect the gain pattern amplitudes due to multipath. We conducted simulation and empirical experiments, which reveal that when an unobstructed line-of-sight path exists, the energy variations of the gain pattern due to multipath are minimal. This scenario is common in outdoor spaces and certain

large indoor spaces (e.g., warehouses). To validate our hypothesis, we conducted a simulation study and observed that the energy contrast between the direct path and reflected paths is extremely high, owing to the losses incurred by the inverse-square of the distance factor and the absorption of the signal by reflecting surfaces. The gain pattern of the received signal, as demonstrated in Figure 5, reveals that the direct path accounts for 92% of the energy, while all reflections combined constitute only 8% of the total energy. We evaluate *Sirius*'s performance in different levels of multipath and non-line-of-sight (NLOS) scenarios in the evaluation section, where we discuss the effectiveness of AoA estimation under such conditions. We conclude that if the direct path accounts for 80% of the signal energy, then gain codes can be effectively employed to extract the AoA.
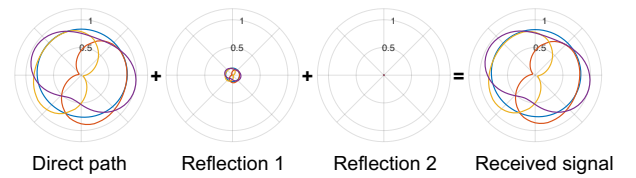

Figure 5: Gain patterns for the first 3 paths that signal takes to reach the antenna. First one is the direct path which constitutes the majority of the energy, followed by weaker reflections.

3.3 Localization with Independent Beacons

Sirius uses the triangulation method for localization, which requires angle estimations from at least two known anchor locations as shown in Figure 6. We aim to make the localization process independent of the communication to the access points (AP). This allows our system to operate in parallel to any unmodified communication protocol using the same receiver radio and *Sirius* antenna. We rather use two or more unsophisticated narrowband beacons as the anchors without any synchronization. These anchor-beacons require a one-time parameter selection setup and their hardware consists of simple oscillator-based frequency generators, which further reduces the cost and power consumption for long-term maintenance-free deployment in scale. However, this simple localization infrastructure requires addressing two challenges on the ultra-low-power receiver node: (a) identification of signals from individual anchor-beacons and (b) detecting and avoiding collisions of unsynchronized beacons signals.

To make sure that the node receives the signal from each anchor beacon without interference, we design the transmitting signal using On-Off keying. Our key observation is that if the duty cycle of the anchor signals is different from each other, then no matter what time offsets they have, there will be a repeating time window in the received signal where only Anchor1 and Anchor2 signals are received. Additionally, if we set the duty cycle of Anchor1 equal to twice that of Anchor2, then it results in equal time windows for both anchors. Figure 8 shows the received signals in different cases of time offsets between the anchors.

Anchor identification: Let us assume that we have an algorithm to detect collision windows, which we will explain later. Our core
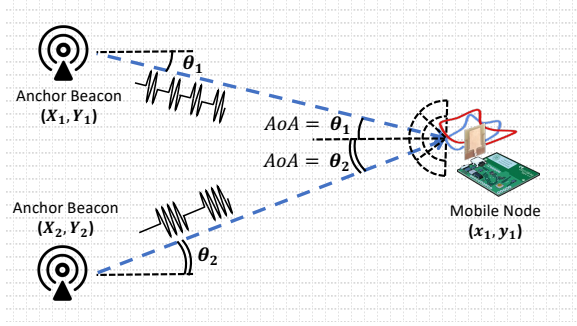
Figure 6: *Sirius* uses triangulation to localize mobile nodes.
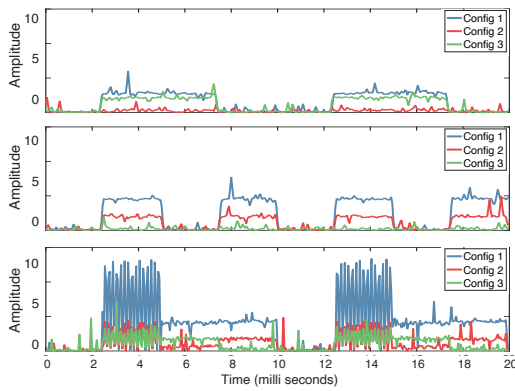It estimates angles from at least two anchors with known
locations.

Figure 7: Figure depicts envelope detector's received signal:
(top) Anchor1 transmitting, (middle) Anchor2 transmitting,
and (bottom) both Anchor1 and Anchor2 transmitting.

idea here is that if the duty cycle of the anchors are set, then no
matter what the time offset is, there can only be two possible cases of
collisions. Case 1, where the length of collision is equal to anchor1's
time period, and Case 2, where it is smaller than anchor1's time
period. Figure 8 shows both cases where collisions are represented
by a sinusoid wave.

Our algorithm first aims to identify the case of collision (Case 1
or Case 2) by looking at the length of the collision windows. We
empirically found that a tolerance threshold of 95% works best
to identify the collision case. After the identification of the type
of case, we assign the exterior neighbors of collision windows as
anchor2 and interior neighbors as anchor1 if Case 1 is detected.
Whereas, if Case 2 is detected, we assign the interior neighbors of
collision windows as anchor2 and exterior neighbors as anchor1.

Identifying collisions: If we successfully find the collision
window, then the Anchor detection algorithm can label time
windows to their corresponding anchors. However, detecting
collisions is not straightforward in *Sirius* because we do not sample
the incoming signal. As discussed in the previous section, we use an
envelope detector which only gives the amplitude of the incoming
signal. To solve this challenge, we leverage the non-linear properties
of the envelope detector. We transmit a single tone of frequency,
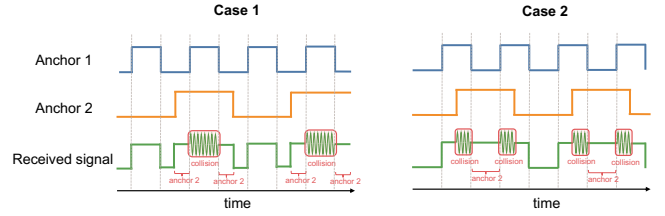f_1 from anchor1 and, a slightly different frequency, $f_2 = f_1 + \Delta f$

Figure 8: Anchor beacon signals designed with varying duty
cycles create distinct time windows for interference-free re-
ception. (left) Case 1: Anchor2's window as the outer neigh-
bor of collision windows. (right) Case 2: Anchor2's window
as the inner neighbor of the collision window.

from anchor2. Due to the non-linear property of the rectifier, the
output contains a beat frequency component equal to Δf. Let us
take a closer look at this.

Let $x_1(t) = A_1 e^{j2\pi f_1 t}$ and $x_2(t) = A_2 e^{j2\pi f_2 t}$ be two sinusoidal
signals with frequency f_1 and f_2 be transmitted from the two anchor
beacons respectively. When received by *Sirius*'s receiver antenna,
the signal will become a superimposition of $x_1(t)$ and $x_2(t)$ which
can be written as

$$y(t) = A_1 e^{j2\pi f_1 t} + A_2 e^{j2\pi f_2 t} \tag{4}$$

$$y(t) = [A_1 e^{j2\pi(\frac{f_1-f_2}{2})t} + A_2 e^{-j2\pi(\frac{f_1-f_2}{2})t}]e^{j2\pi(\frac{f_1+f_2}{2})t} \tag{5}$$

In other words, $y(t)$ is an amplitude modulated signal with
modulation frequency $\frac{f_1-f_2}{2}$ and carrier $\frac{f_1+f_2}{2}$.

After the envelope detector, the output signal, $y_{env}(t)$, becomes the
absolute of $y(t)$

$$y_{env}(t) = |y(t)| = |A_1 e^{j2\pi f_1 t} + A_2 e^{j2\pi f_2 t}| \tag{6}$$

$$y_{env}(t) = A_1^2 + A_2^2 + 2A_1 A_2 cos(2\pi(f_1 - f_2)t) \tag{7}$$

We clearly see that in the case of superimposition, or collision, a
beat frequency, $\Delta f = |f_1 - f_2|$ appears in $y_{env}(t)$. Figure 7 shows
time domain signals collected in the real world where the beat
frequency is shown due to the collision of anchor signals.

Note that Δf is hardly affected by the clock drifts of unsynchronised
beacons. A typical 10Mhz oscillator drifts at a rate of $2-6ppm$ [1, 4].
For $\Delta f = 10kHz$ centered around 2.4GHz, the frequency can be
deviated by only $500 - 600Hz$ which is a negligible difference (<6%)
in the beat frequency. We have also shown the impact of clock drifts
and frequency offsets on *Sirius* in the evaluation section.

Beat frequency detection: We use a sliding window to classify
each window as "No signal", "Signal detected" or "Collision detected".
We first apply a threshold on the signal energy to identify if the
received signal has at least one anchor's signal and label it as "Signal
detected". Then we apply a beat frequency detection algorithm to
identify collision regions and label them as "Collision detected".

To make a robust beat frequency detector, we leverage
synchronization in antenna configuration switching. We sample
all the configurations in a burst, which makes the signals from the
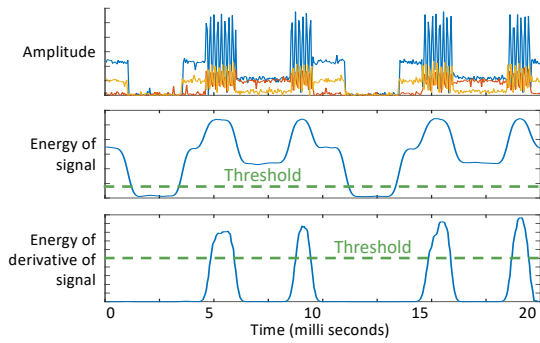antenna configuration synchronous. To identify a beat frequency,

Figure 9: Figure displays anchor detection algorithm outputs: (top) time domain signal, (middle) total energy from all configurations, and (bottom) signal's first derivative.

we find the first derivative of the signal by taking the difference between adjacent samples. In the case of DC, the result is zero, but an oscillating signal is preserved with only DC bias removed. We find the energy of this oscillating signal around zero by taking an absolute sum. Figure 9 shows the steps of finding beat frequency. Due to some nulls and low gain points in the gain pattern, the beat frequency might be weak and hard to detect. To solve this, we also take the product of the energy obtained from all the configuration signals. This suppresses false positives and amplifies the beat frequency confidence value. Then we simply apply a threshold to identify if the time domain window is a collision or not.

3.4 Designing Programmable Directional Gain

The main focus of designing the antenna is to have a reconfigurable and programmable gain pattern. The gain pattern is determined by various characteristics like the patch shape, feed locations, and substrate parameters of the antenna. The most efficient way to make a single antenna reconfigurable is to change its shape. We use switches to connect or disconnect patches of conducting elements to the antenna. Depending on the location of these patches, it alters the flow of current inside the antenna. This changes the gain pattern as shown in Figure 2. However, adding a random patch to the antenna can lead to impedance mismatch and decrease the sensitivity of the antenna. We use HFSS simulation to carefully design the antenna and tune the location and shape of each additional patch. We design reconfigurable antennas in two ISM bands (900MHz and 2.4GHz) to show that the antenna can be tuned to any desired frequency while achieving reconfigurable gain patterns. In our system, we use pin-diode-based RF switches which only require two different voltage levels (e.g., 0V or 3V) to toggle between open and closed states. The switches are located on the antenna surface between the patches. We control the state of the switch using dc voltage which is applied from an external microcontroller.

3.5 Pin-diodes as RF Switches

Pin diodes, unlike conventional diodes, act like current-controlled resistors for microwave frequencies. The value of resistance is set by the DC current flowing through the diode. The PIN diode behaves like a closed circuit in forward bias, when current is flowing through it, and has a very high resistance to microwave frequencies
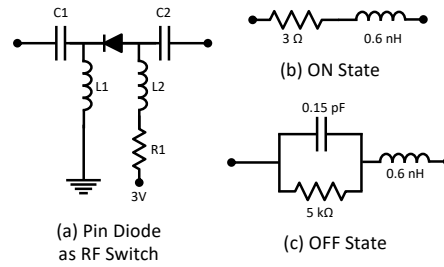

Figure 10: Using pin diode as RF switch. (a) Biasing circuit (b, c) Equivalent lumped model for on and off states.

otherwise. We can control the state of the switch by applying a constant voltage across the two terminals of the diode as shown in Figure 10(a). We limit the amount of current flowing through the diode using a resistor, $R1$. Figure 10(b) shows the equivalent lumped circuit model of the pin diode in On and Off states. In forward bias, which is the on state, the PIN diode is modeled as an inductor and resistor in series. In off-state, it is modeled as an inductor in series with a paralleled capacitor and resistor. As shown in the figure, we use 3Ω, $0.6nH$, $0.15pF$ and $5k\Omega$ as our values to model the lumped components. These values are obtained from the datasheet [27] provided by the manufacturer.

Pin diodes are two-terminal devices and using them as a switch requires merging the control terminals with the RF terminals. This merging leads to a problem of RF signal leaking out of the antenna. The switching circuit and wires become a part of the antenna and contribute to signal reception and transmission, which affects the overall gain pattern of the antenna. To isolate the biasing circuit from the RF terminals, we use inductors and DC-blocking capacitors. The capacitors prevent the DC bias current from entering the antenna and the inductors act as RF chokes which prevents the RF signals from passing through the switching circuit while providing a clear path for the DC bias current. Figure 10(a) shows the biasing circuit with the isolating components.

• Can *Sirius* antenna be used for communication?

A lot of works on low-power IoT use an envelope detector-based radio receiver to reduce power consumption. *Sirius* aims to complement these IoT systems with spatial sensing and localization.
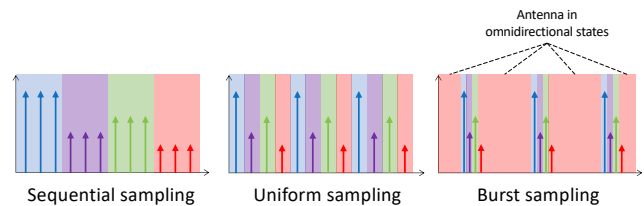

Figure 11: Switching and sampling techniques: (a) Sequential sampling: constant-time switch, hold, and sample, (b) Uniform sampling: continuous configuration switching with constant rate, (c) Burst sampling: high-speed switching and sampling with long duty cycles for omnidirectional communication.

We aim to design the sensing pipeline in such a way that any existing communication pipeline is unaffected by the amplitude fluctuations introduced due to gain pattern switching.

One of the core challenges in designing such a pipeline is to switch the antenna configuration fast enough. Low-speed switching hinders the communication abilities of the antenna since changing the configuration of the antenna can also affect the wireless channel. As we discussed in the previous section, *Sirius* uses pin diodes as switches instead of conventional RF switches. The fast response time of pin diodes enables us to switch the antenna configuration at extremely high speeds. In our prototype, we have used the Infineon BAR50-02v [28] pin diode that can change its state in less than 1.1 microseconds, achieving a maximum switching rate of 1MHz.

We leverage this high-speed switching of pin diodes to sample the signal in bursts. As shown in Figure 11 traditional sampling techniques either use sequential sampling i.e., sampling one configuration at a time, or uniform sampling i.e., continuously switching the configuration and sampling. Both techniques require repeated changing of the configuration which constantly disturbs the wireless communication channel. In burst sampling, we keep the antenna in a default state where both the switches are off and the antenna has an omnidirectional gain pattern. This consumes no energy since the switches are off and the antenna behaves like a regular antenna. When the system needs to find the AoA it switches the antenna configuration in a fast burst fashion and collects one sample at each configuration. This burst switching repeats at a time period defined by the user. Due to the extremely high-speed switching rate of pin diodes, the antenna can stay in the default omnidirectional state for the majority of the time, which can lead to uninterrupted communication. We evaluate the communication quality later in the evaluation section.

3.6 Directional Code to AoA Mapping

Sirius embeds directional codes by dynamically switching the gain pattern of the antenna. These codes are unique for each angle and thus map to a specific angle-of-arrival. In our design process, we first design the antenna in HFSS simulation and optimize the diversity of all gain pattern configurations. In an ideal system, we should use the simulated gain patterns to learn and store the mapping function from the extracted codes to angles. However, due to imperfections in real-world fabrication process and assumptions in antenna modeling, the simulated gain patterns might not match with the measured gain patterns, which leads to errors in AoA estimation.

Therefore, in *Sirius*, we do a *one-time* calibration and record the real gain patterns of the antenna. We perform the calibration only once, which can be used for all the other antennas fabricated with the same parameters and materials. In other words, for *Sirius* to become a product, the manufacturer only needs to calibrate once and produce multiple antennas using the same calibration data.

There are multiple ways to store and learn the mapping function from extracted codes to angles. For example, one can use look-up tables, euclidean distance-based estimation, SVM or neural networks to find the angles. In our experiments, we compared the

euclidean distance-based method and the neural network-based method. We found that neural networks are robust to environmental changes even though they consume more power for computation. We also show the performance results of euclidean distance-based system in section 4.5.

In *Sirius*'s prototype, we train a small multilayer perceptron with 4 fully connected layers of size 16x8x16x1. Each layer is followed by a relu activation function to capture the non-linear gain patterns and the last layer is a softmax regression layer to estimate the angle in degrees. To reduce the power consumption of computation, we optimize the inference operations for a low-power microcontroller. We use the Low-Energy Accelerator (LEA) library provided by MSP430 [29]. The library supports dot multiplication of matrices, which accelerates forward propagation. We also developed a tool in Matlab that can take any trained model as an input and produce a header file in C containing the architecture of the model, the learned weights and biases, and the functions required for the angle inference. We will also open-source this tool for the community along with the other source codes of *Sirius*.
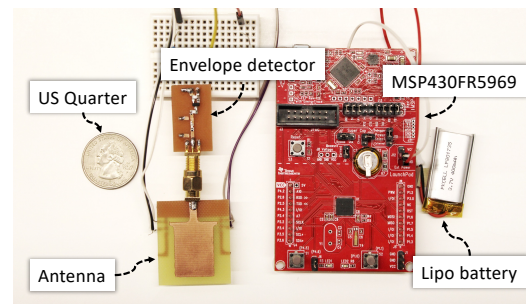

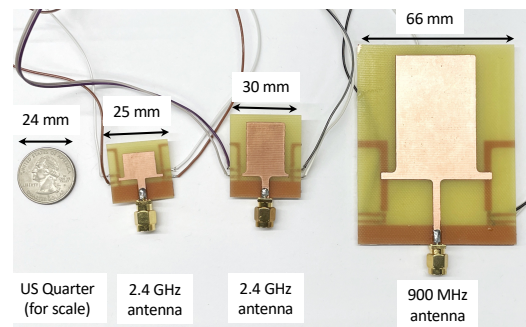**Figure 12:** *Sirius***'s prototype for localization.**

Figure 13: We evaluate *Sirius* on different antennas in ISM band 900MHz and 2.4GHz. The figure shows the fabricated reconfigurable antennas used in the prototype.

4 EVALUATION

To this end, we implement a prototype of *Sirius* and evaluate the key components.

Node setup: Figure 12 shows the implemented prototype of our mobile node. It consists of a reconfigurable antenna, an envelope detector, and a low-power microcontroller. The microcontroller
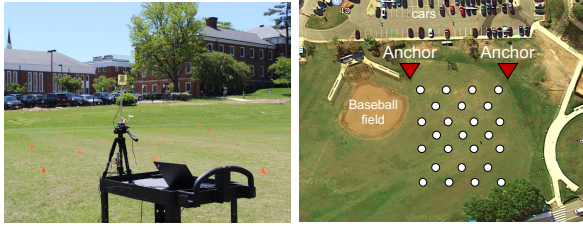
Figure 14: Setup for outdoor long-range data collection. The map shows the static anchors and node locations.

Figure 15: (a) Overall AoA estimation accuracy of *Sirius*. (b) CDF of AoA error.

takes care of switching the gain pattern of the antenna and sampling the output voltage of the envelope detector. We have used MSP430FR5969 [30] as our microcontroller due to its low power footprint and optimized LEA library [29] for matrix multiplication. Figure 13 shows the lineup of fabricated antennas centered at 900MHz and 2.4GHz. The antennas are designed and optimized using HFSS simulation software [5] and etched on FR4 PCB. Each antenna consists of two pin diodes, one on each side of the antenna, acting as RF switches. The circuit diagram of the RF switch is shown in Fig 10, where R1 is a 100ohm resistor, L1 and L2 are 200nH chokes, and C1 and C2 are 100pF DC blocking capacitors. We used the Infineon Bar50-02v [28] as the pin diodes since they have a very fast switching speed and low insertion loss. The antenna is directly connected to the envelope detector which is a single-stage dickson rectifier consisting of two Skyworks SMS7630 schottky diodes [59]. To increase the efficiency of the envelope detector, an impedance matching network is used to match the input impedance of the circuit to 50Ω impedance of the antenna.

Anchor beacon setup: In the performed experiments we have used the following configuration. We use the SDR, USRP N210, as our transmitting anchor beacons. The output of the SDRs are connected 3dBi omnidirectional antennas Ettus VERT900 [12] and VERT2450 [13] for 900MHz and 2.4GHz experiments respectively. We use a power amplifier RF5110G [54] and tune the output power to 30dbm which is within the allowed power limits by FCC.

4.1 AoA Performance

To perform controlled AoA experiments, the antenna was mounted on top of a programmable turntable controlled by an arduino and a stepper motor. We used MATLAB to communicate with the turntable and control the precise rotation of the antenna. Finally, the output from MSP430 was communicated to MATLAB using a USB-to-serial interface and stored for evaluation. We performed the experiment outdoors for varying locations and environments throughout the measurements. Fig. 15(a) shows *Sirius*'s overall performance in estimating AoA. The figure presents the average estimated angle at each measurement along with error bars indicating standard deviation. 15(b) shows the cdf of the overall error. The median AoA error is less than 7 degree.

4.2 Localization

We evaluate the localization performance of *Sirius* in a long-range outdoor environment which is closer to real-world deployment.
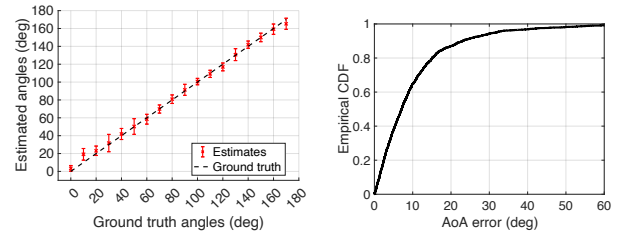
The experiments are conducted in an open field surrounded by multiple trees on the boundary, and a parking lot with multiple cars. The setup used in this evaluation is similar to the previous experiment. We place our mobile node on a portable cart to emulate a moving vehicle or a drone. Fig. 16(a) shows the setup in the open field. We place two AP in the field and move the cart to the marked locations shown in Fig. 16(b). The maximum distance between the AP and the node was 26 meters. We collect the estimated locations for all the possible orientations of the receiving antenna at all the marked locations. Figure 16(c) shows the CDF of the estimated AoA error. The median error in location is less than 2.5 meters while the error in 1D localization is less than 1.3 meters.
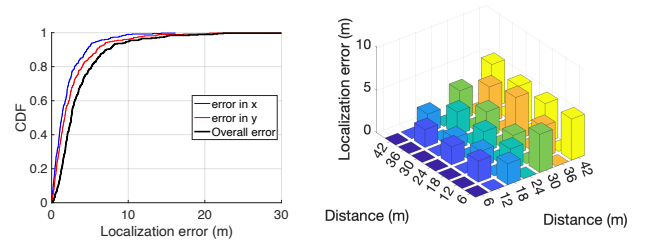

Figure 16: (a) CDF of localization error (b) Localization error per location shows the impact of distance from the APs.

4.3 Impact on RF Communication

We evaluate the ability of *Sirius* to support wireless communication along with angle-of-arrival estimation. *Sirius* uses a reconfigurable antenna that repeatedly changes the gain patterns of the antenna. This can lead to disruption in communication due to changes in the effective channel. To evaluate the impact of switching, we set up an experiment using our antenna as a receiver and a COTS 900MHZ antenna, VERT900 [12] as the transmitter antenna. Both antennas are plugged into the SDR USRP-N210 [14] interfaced with Matlab. The transmitter USRP device continuously transmits messages at a bit rate of 2Mbps and the receiver USRP calculated the total number of bit errors while addressing problems such as carrier frequency offset, timing offset, and frame synchronization [47]. The modulation used in this experiment was QPSK of order 4. While receiving the messages, we run *Sirius* system with varying rates of switching using an MSP430. Figure 17 shows the effect of beam pattern switching on BER. We observe that even at switching speeds of 480 configurations per second, the BER is < 0.001. Figure 18 compares the BER of our antenna with the COTS antenna. We observe that our antenna running at 100Hz of AoA has a similar BER with the COTS antenna.
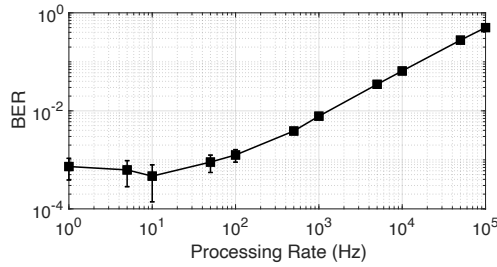
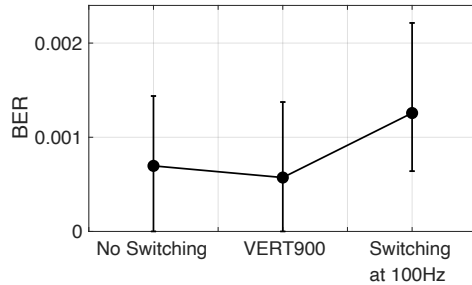**Figure 17: Effect of pattern switching speed on communication.**

Figure 18: Impact of antenna reconfiguration on bit error rate for different antennas.

4.4 Power Consumption

In this section, we benchmark the power consumption of *Sirius*'s prototype. We measure the energy consumption of each sub-module of the system. Table 1 shows the breakdown of the energy consumption for one location estimation. The switching and sampling sub-module consists of the energy consumed by the pin diode-based RF switch and ADC and of the microcontroller. The beacon detection algorithm consumes the least energy and it consists of rearranging the samples of different antenna configurations and classifying the signal to corresponding anchor beacons. The AoA estimation sub-module is the forward propagation of a floating point precision neural network. We run the AoA sub-module once for each beacon to get the x and y coordinates. The total energy consumed per location estimate is $36mJ$.

Submodule	Energy consumed
Switching and sampling	$0.32mJ$
Beacon detection	$0.09mJ$
AoA estimation	$19.50mJ$
Total energy per AoA	$19.81mJ$
Total energy per Location	$36.71mJ$

Table 1: Breakdown of energy consumption.

4.5 Robustness

In this section, we evaluate the robustness of *Sirius* in varying practical conditions like varying level of multipath, NLOS cases, number of gain patterns, reflections material, clock drift, frequency deviations, and distance from the anchor beacons.

Impact of multipath: *Sirius* assumes that the line-of-sight path (direct path) exists between the transmitting beacon and the
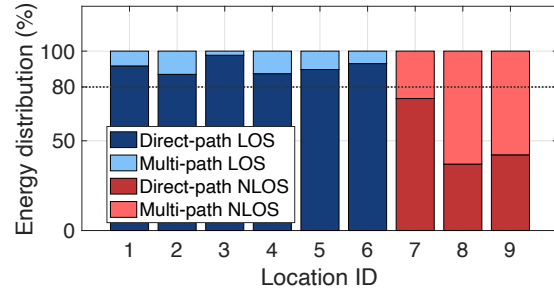

Figure 19: Energy distribution between direct path and multipath for various indoor locations.

receiving antenna. However, due to the presence of reflecting surfaces in the environments, the radio signals also reflect multiple times before reaching the antenna through other paths. Due to the loss of energy during propagation, reflections, and absorption, radio waves undergo exponential attenuation. Since the magnitude of attenuation is proportional to the inverse square of the distance traveled and the number of reflections, the energy contrast between the direct path of the signal versus the reflected paths is extremely high. We perform an extensive simulation study, using the RF communication toolbox in Matlab [46], in various multipath scenarios to analyze the energy distribution of the signal between the direct path rays and multipath rays. Figure 19 shows the distribution of the energy between these two types of paths as percentages. We clearly see that in LOS cases when the direct path is unobstructed, more than 80% energy is concentrated in the direct path. However, in NLOS scenarios, the direct path becomes weaker and the contrast of energy decreases to less than 50%. This impacts the overall AoA estimation errors.

Impact of NLOS: To compare *Sirius*'s performance in LOS and NLOS scenarios, we simulate both scenarios. The LOS cases have a clear direct path between the transmitting beacon and the receiver, whereas NLOS cases have an obstacle like a wall or a furniture item between the direct path. Figure 20 shows the median errors in the AoA estimation for both scenarios. The results indicate that *Sirius* can estimate angles within 10 degrees of median error in all 6 LOS locations. However, in NLOS scenarios, where the reflections overpower the direct path's energy, the estimation errors increase up to 50 degrees.

Impact of reflection surface material: A significant portion of energy loss occurs during the reflection of radio waves from an object. The relative permittivity and conductivity of the material of these objects determine the amount of radio signal which gets
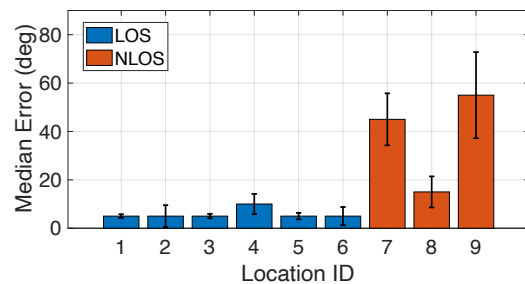

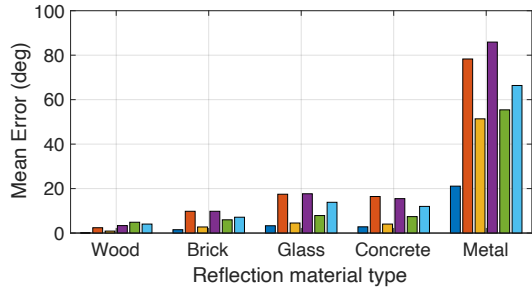**Figure 20: AoA errors for different indoor locations.**

Figure 21: AoA errors for different reflection materials. Each cluster of bars represents one type of material, and each bar within a cluster represents different indoor locations.

absorbed and reflected. To study the impact of this material type, we simulate the five most common types of material found in an indoor environment and run simulations at various indoor locations. Figure 21 shows the mean AoA estimation errors for wood, brick, glass, concrete, and metal.

Impact of dynamic environment: Since the performance of *Sirius* depends on the movement of reflecting surfaces and multipath signals, we perform a real-world evaluation in three different levels of dynamic multipath, as shown in Figure 27. We conducted low dynamic level experiments in an outdoor environment, adjacent to a glass building with 2-3 people moving around. Medium dynamic-level experiments were carried out in an indoor hall with 5-10 people around, while high dynamic-level experiments were also conducted in the same indoor hall but with a large crowd (>20 people) moving around naturally. Figure 23 shows the mean AoA error in increasing level of dynamic levels. We clearly see that when the environment is less dynamic, the AoA error is low with limited standard deviation. However, in more dynamic conditions, where the reflection paths fluctuate in close proximity, the mean AoA errors increase up to 20 *degrees*.
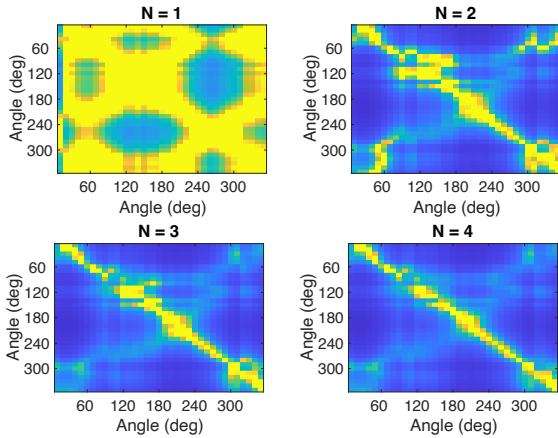

Figure 22: Inverse distance matrix for varying number of gain patterns (N).

Impact of number of patterns: *Sirius* aims to achieve ideal diversity by optimizing for a diagonal distance matrix of gain-pattern features. In this experiment, we investigate the impact
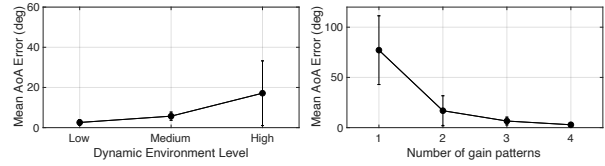

Figure 23: AoA estimation errors. (left) varying levels of multipath density in the environment. (right) varying number of gain patterns.

of the number of switches and gain patterns on overall diversity and AoA estimation accuracy. Specifically, we examine the correlation between the number of gain patterns, diversity, and AoA estimation errors. As depicted in Figure 22, we observe that increasing the number of reconfigurable gain patterns leads to a larger distance between the features and nearby angles. Notably, the confusion matrix displays a faint diagonal, indicating ambiguity in 180-degree apart angles, such as 120 and 300 degrees (i.e., 120+180). This confusion is more frequent in angles where the on-off and off-on are similar. However, as we increase the number of switches, the ambiguity decreases, resulting in a more accurate estimation. Figure 23 shows the mean AoA estimation accuracy for varying number of gain patterns. The error sharply drops as we increase the number of patterns from 1 to 3 and then it slowly saturates as the change in diversity is not as much.

Long term stability: Figure 24 shows the temporal stability of the antenna gain patterns over 72 hours. Our experiment tested the system every 24 hours for 360 degrees of AoA estimation at 10-degree steps in an indoor environment with the natural movement of people and furniture. Figure 24 (a) presents the correlation metrics for gain patterns at varying time intervals, while Figure 24 (b) shows mean and median AoA estimation results. We conclude that the gain patterns are predictable and stable for long time intervals.
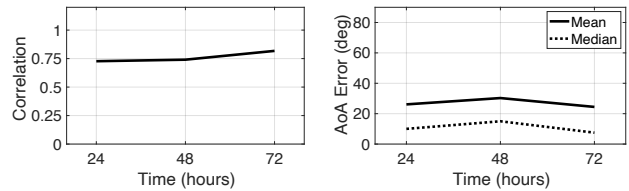
(a) Gain pattern correlation   **(b) AoA estimation results**

Figure 24: (a) Correlation of gain pattern amplitudes. (b) Mean and median AoA errors showing the long-term stability of gain patterns in a dynamic environment.

Indoor vs outdoor: We also compare the performance of AoA estimation in indoor vs outdoor setups. We record the gain pattern of the antenna at multiple indoor locations to see the effect of multipath on the gain pattern. Figure 25 shows an example of the gain patterns in two different indoor locations. We show the setup for this experiment in Figure 27. We also evaluate the AoA performance in indoor vs outdoor setups. Figure 26 shows the CDF of AoA error. We clearly see that *Sirius* performs equally well with a median AoA error of 7-8degrees in all environments.
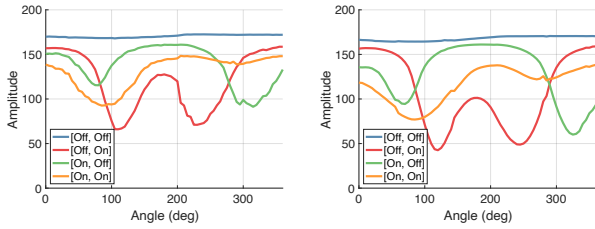
Figure 25: The figure shows gain patterns collected at two different indoor locations in a dynamic environment.
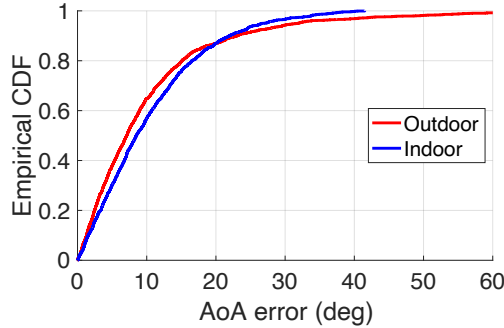

Figure 26: CDF of AoA error for different environments.

Figure 27: Our experimental setup at different indoor locations in varying levels of static and dynamic multipath.

Impact of distance: Increasing the distance between the anchor beacon and the node changes the incoming signal strength and the absolute gain pattern. We evaluate its impact on the AoA performance. Figure 28 shows the median error in AoA for varying distances. Even though the absolute gain pattern changes, the relative gain pattern still remains the same. The median error is 7 degrees with a standard deviation of 3 degrees.
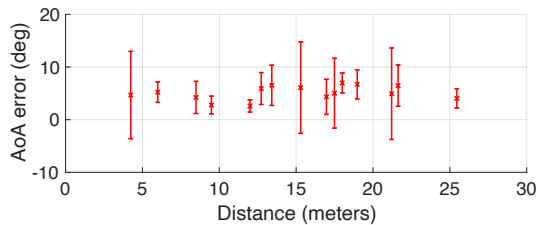

Figure 28: AoA error for varying distance from the anchor.

Impact of clock drift: We evaluate the effect of unsynchronized clocks on AoA error. To see the impact of clock drift we collect data over a period of five hours without any external reference clock. We find the average drift as 5-7ppm. Figure 29 shows the confusion matrix of euclidean distance-based estimation between the two sets

of gain patterns collected in five hours. We also show the spectrum of an example test signal where we clearly see the peak.

Impact of frequency shift: Perceived frequency of a node can be different from the transmitted frequency due to various reasons like doppler effect, carrier frequency offset, or clock drift. In this evaluation, we test the impact of any frequency shift on the gain pattern. We collect a set of gain patterns for 2.400GHz and 2.401GHz (1MHz difference). Figure 30 shows the confusion matrix between the two frequencies. We see a strong correlation between the two gain patterns. Even a euclidean distance-based estimation gives us a 10deg median error.

5 LIMITATION AND FUTURE WORK

NLOS scenarios: Despite its promising performance, *Sirius* has a limitation of assuming the existence of a line-of-sight (LOS) path between the transmitting beacon and the receiving antenna. This assumption may not always hold true due to the presence of obstacles in the environment. To overcome this limitation, one possible solution is to extract the channel impulse response and pick the first peak corresponding to the direct path signal. However, implementing this solution in low-power hardware would require significant innovation, which we leave to future work.

Dense multipath: Through our experiments in dense indoor environments, we have found that *Sirius* can successfully estimate the angle of arrival if the direct path energy accounts for at least 80% of the total energy. However, this condition may not hold true in scenarios with extremely closely placed reflectors or near-perfect reflecting surfaces, where the proportion of direct path energy may decrease, leading to higher AoA estimation errors.

Accuracy and power consumption tradeoff: While increasing the number of gain-pattern configurations improves diversity and accuracy, it also requires more pin diode switches, leading to increased power consumption. Alternatively, one could employ low-power methods to configure antennas such as switching feed points or polarization [44, 49]. Our evaluation results demonstrate that, with up to 480 reconfigurations per second, the bit error rate (BER) of a communication link remains below 0.001.

6 RELATED WORK

We have summarized the related works in Table 2.

RF Localization: The topic of RF Localization has received a lot of attention from the academic community over the past years. Most of the works either rely on either ranging [39, 55, 68, 73] or angle-of-arrival [38, 62, 71, 72] to localize a node. However, achieving good accuracy has required complex systems architectures like large antenna arrays or tight time synchronizations for extracting phase information. The AoA resolution is limited by the number of antennas in the arrays and their separation distance. Some papers [39, 45, 76] have emulated an array of virtual antennas by leveraging the motion of the node. *Sirius* proposes a miniaturized *single-antenna* system that can estimate AoA with multiple APs without requiring any kind of synchronization. *Sirius* uses a passive envelope detector and low-power ADCs to sample the energy of the signal. *µ*Locate [50]

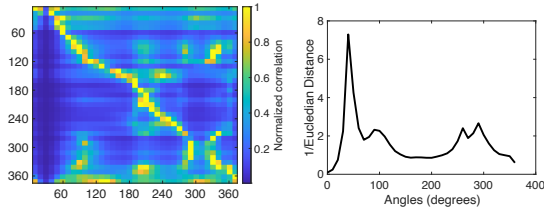| Past work	Self-localization	Single-antenna node	Single-antenna anchor	Low-power	Synchronization-free	Accuracy
[39, 55, 68, 73]	✗	✓	✓	✗	✗	50 cm
[38, 62, 71, 72]	✗	✓	✗	✗	✓	6 degrees
[34]	✓	✗	✓	✗	✓	7.5 cm
[33]	✓	✓	✗	✓	✗	4.6 degrees
Sirius	✓	✓	✓	✓	✓	7 degrees

Table 2: Summary of related work.

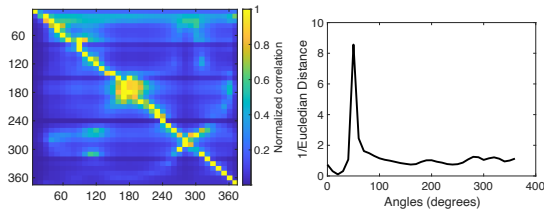Figure 29: Impact of clock drift on AoA estimation

Figure 30: Impact of frequency shift on AoA estimation

and TagFi [60] backscatter RF signals from a low-power tag and receive from one or more APs to estimate the location. This provides an energy-efficient way to localize multiple low-power nodes but the location is estimated on the AP side which limits the scalability. Moreover, the SNR of backscatter signal is weaker compared to active radios which limit its application to small-range indoor environments. RFID-based works like RF-IDraw [69] use antenna arrays to find the angle-of-arrival of the tag and RFind [43] shows that RFID tags can backscatter wide bandwidths, up to 220MHz, to achieve fine-grained resolution ranging. While RFID tags consume less power they do not have the resources to do self-localization and their ranges are limited to 3-6 meters.

RF Self-localization: Living IoT [33] designs a self-localization system that can be attached to bumblebees. Similar to *Sirius*, LivingIOT uses multiple APs and angle-of-arrival to find the location of the node. However, the technique uses AP beamforming at the AP which requires multiple antennas. Moreover, all the APs must be time synchronized with each other and with the nodes to avoid interference. *Sirius* uses a single antenna and does not require any synchronization. This allows the system to be easily deployed in remote locations. *Sirius* also differs from [33] in localization latency and fast mobility. LivingIOT system takes $100ms$ to sweep the AP beams and one location. This limits the node's mobility relative to the APs. *Sirius* tackles this problem by using high-speed pin diode-based switches which can go up to 10^3 AoAs/second without trading off the communication link. ISLA [34] proposes a self-localization system that leverages the high bandwidth of 5G signals to perform better ranging. It leverages MEMS acoustic resonators instead of high-speed ADCs to improve the ranging resolution. ISLA differs from *Sirius* as it is a time-of-flight-based technique whereas *Sirius* is an angle-of-arrival-based technique.

ISLA nodes have two receiving antennas on the node and consume high power because of the bulky RF front end. In *Sirius* the nodes have a single antenna and an envelope detector and use no power-consuming front end like clocks and down converters, which dramatically reduces energy consumption.

Reconfigurable antennas: The applications of reconfigurable antennas is multi-fold. An antenna can be reconfigured in frequency [22, 26], gain pattern [2, 42, 52], polarization [3, 65, 70] or a combination of all [8, 9, 51, 53]. In prior works, researchers have used multiple ways to reconfigure antennas. [11, 41, 48, 56] use actuators and motors to physically change the structure or shape of the antenna. [24, 26, 52] uses electrical switching to connect or disconnect patches to the radiating surface of the antenna. RF-MEMS switches [10, 23, 74, 77] use mechanical movement which gives good isolation and insertion loss, however, they have high power consumption. Pin-diodes based switching [22, 26, 31, 35, 52] offer low power footprint and are very fast, in order of nanoseconds. The idea to use reconfigurable antennas for angle-of-arrival estimation has been explored in [24, 25, 36, 64]. However, existing works require sampling of IQ samples of the signal. Whereas, *Sirius* uses an envelope detector to only sample the energy of the signal. Moreover, most of the system implementations are limited to simulation models and anechoic chamber experiments. [31] is the closest work with *Sirius* in terms of antenna design since both the works use monopole antenna design and pin diodes to switch the configuration. However, [31] is a composite frequency and pattern reconfigurable antenna tuned to operate at 3.1 GHz and 6.8 GHz. In our prototype, we design the antenna at 900MHz and 2.4GHz ISM bands.

7 CONCLUSION

This paper presents *Sirius*, a low-power self-localization system. The core idea of the paper is to embed directional codes to any received signal by dynamically switching the gain pattern of an antenna. The received signal carries the code in amplitude fluctuations which uniquely maps to the angle-of-arrival. *Sirius* develops a robust AoA estimation technique using envelope detector-based receiver and creates a prototype for demonstration and performance evaluation. Our evaluations show a median AoA error of less than 7degrees of localization error of 2.5meters while consuming only 19mJ and 36mJ of energy for the respective modules. The paper breaks away from traditional array-based AoA methods and opens up new possibilities for low-power IoT nodes.

8 APPENDIX

The research artifact accompanying this paper is available via https://doi.org/10.5281/zenodo.7922283

REFERENCES

[1] Omid Abari, Hariharan Rahul, Dina Katabi, and Mondira Pant. Airshare: Distributed coherent transmission made seamless. In *2015 IEEE Conference on Computer Communications (INFOCOM)*, pages 1742–1750. IEEE, 2015.

[2] Tamer Aboufoul, Clive Parini, Xiaodong Chen, and Akram Alomainy. Pattern-reconfigurable planar circular ultra-wideband monopole antenna. *IEEE Transactions on Antennas and Propagation*, 61(10):4973–4980, 2013.

[3] Yasir IA Al-Yasir, Abdulkareem S Abdullah, Naser Ojaroudi Parchin, Raed A Abd-Alhameed, and James M Noras. A new polarization-reconfigurable antenna for 5g applications. *Electronics*, 7(11):293, 2018.

[4] Kubra Alemdar, Divashree Varshney, Subhramoy Mohanti, Ufuk Muncuk, and Kaushik Chowdhury. Rfclock: timing, phase and frequency synchronization for distributed wireless networks. In *Proceedings of the 27th Annual International Conference on Mobile Computing and Networking*, pages 15–27, 2021.

[5] Ansys. https://www.ansys.com/products/electronics/ansys-hfss, 2022.

[6] Yang Bai, Nakul Garg, and Nirupam Roy. Spidr: Ultra-low-power acoustic spatial sensing for micro-robot navigation. In *Proceedings of the 20th Annual International Conference on Mobile Systems, Applications and Services*, pages 99–113, 2022.

[7] Yang Bai, Nakul Garg, and Nirupam Roy. Ultra-low-power acoustic imaging. In *Proceedings of the 20th Annual International Conference on Mobile Systems, Applications and Services*, pages 523–524, 2022.

[8] Jennifer T Bernhard. Reconfigurable antennas. *Synthesis lectures on antennas*, 2(1):1–66, 2007.

[9] Marta Cabedo-Fabres, Eva Antonino-Daviu, Alejandro Valero-Nogueira, and Miguel Ferrando Bataller. The theory of characteristic modes revisited: A contribution to the design of antennas for modern applications. *IEEE Antennas and Propagation Magazine*, 49(5):52–68, 2007.

[10] Bedri A Cetiner, Gemma Roqueta Crusats, Lluís Jofre, and Necmi Biyikli. Rf mems integrated frequency reconfigurable annular slot antenna. *IEEE Transactions on Antennas and Propagation*, 58(3):626–632, 2009.

[11] Joseph Costantine, Youssef Tawk, Jonathan Woodland, Noah Flaum, and Christos G Christodoulou. Reconfigurable antenna system with a movable ground plane for cognitive radio. *IET Microwaves, Antennas & Propagation*, 8(11):858–863, 2014.

[12] Ettus. https://www.ettus.com/all-products/vert900/, 2022.

[13] Ettus. https://www.ettus.com/all-products/vert2450/, 2022.

[14] Ettus. https://www.ettus.com/all-products/un210-kit/, 2022.

[15] Ander Galisteo, Ambuj Varshney, and Domenico Giustiniano. Two to tango: Hybrid light and backscatter networks for next billion devices. In *Proceedings of the 18th International Conference on Mobile Systems, Applications, and Services*, pages 80–93, 2020.

[16] Nakul Garg, Yang Bai, and Nirupam Roy. Demo: Microstructure-guided spatial sensing for low-power iot. In *The 19th Annual International Conference on Mobile Systems, Applications, and Services (MobiSys '21)*, 2021.

[17] Nakul Garg, Yang Bai, and Nirupam Roy. Owlet: Enabling spatial information in ubiquitous acoustic devices. In *The 19th Annual International Conference on Mobile Systems, Applications, and Services (MobiSys '21), June 24–July 2, 2021, Virtual, WI, USA*. ACM, 2021.

[18] Nakul Garg and Nirupam Roy. Acoustic sensing for detecting projectile attacks on small drones. In *Proceedings of the 21st International Workshop on Mobile Computing Systems and Applications*, pages 104–104, 2020.

[19] Nakul Garg and Nirupam Roy. Enabling self-defense in small drones. In *Proceedings of the 21st International Workshop on Mobile Computing Systems and Applications. ACM*, 2020.

[20] Nakul Garg, Irtaza Shahid, Erin Avllazagaj, Jennie Hill, Jun Han, and Nirupam Roy. Thermware: Toward side-channel defense for tiny iot devices. In *Proceedings of the 24th International Workshop on Mobile Computing Systems and Applications*, pages 81–88, 2023.

[21] Nakul Garg, Harshvardhan Takawale, Yang Bai, Irtaza Shahid, and Nirupam Roy. Structure assisted spectrum sensing for low-power acoustic event detection. In *Proceedings of Cyber-Physical Systems and Internet of Things Week 2023*, pages 278–284, 2023.

[22] Ricardo Gonçalves, Pedro Pinho, and Nuno B Carvalho. Compact, frequency reconfigurable, printed monopole antenna. *International Journal of Antennas and Propagation*, 2012, 2012.

[23] Alfred Grau, Jordi Romeu, Ming-Jer Lee, Sebastian Blanch, Lluís Jofre, and Franco De Flaviis. A dual-linearly-polarized mems-reconfigurable antenna for narrowband mimo communication systems. *IEEE Transactions on Antennas and Propagation*, 58(1):4–17, 2009.

[24] Mateusz Groth, Mateusz Rzymowski, Krzysztof Nyka, and Lukasz Kulas. Espar antenna-based wsn node with doa estimation capability. *IEEE Access*, 8:91435–91447, 2020.

[25] Aki Hakkarainen, Janis Werner, Nikhil Gulati, Damiano Patron, Doug Pfeil, Henna Paaso, Aarne Mämmelä, Kapil Dandekar, and Mikko Valkama. Reconfigurable antenna based doa estimation and localization in cognitive radios: Low complexity algorithms and practical measurements. In *2014 9th International Conference on Cognitive Radio Oriented Wireless Networks and Communications (CROWNCOM)*, pages 454–459. IEEE, 2014.

[26] Liping Han, Caixia Wang, Xinwei Chen, and Wenmei Zhang. Compact frequency-reconfigurable slot antenna for wireless applications. *IEEE Antennas and Wireless Propagation Letters*, 15:1795–1798, 2016.

[27] Infinion. https://www.infineon.com/dgdl/Infineon-BAR50SERIES-DS-v01_01-en.pdf?fileId=db3a304314dca3890114fea7dd410a92, 2022.

[28] Infinion. https://www.infineon.com/cms/en/product/rf/rf-diode/rf-pin-diode/antenna-switch/bar50-02v/?redirId=192411, 2022.

[29] Texas Instruments. https://www.ti.com/lit/an/slaa720/slaa720.pdf, 2022.

[30] Texas Instruments. https://www.ti.com/tool/MSP-EXP430FR5969, 2022.

[31] Amjad Iqbal, Amor Smida, Nazih Khaddaj Mallat, Ridha Ghayoula, Issa Elfergani, Jonathan Rodriguez, and Sunghwan Kim. Frequency and pattern reconfigurable antenna for emerging wireless communication systems. *Electronics*, 8(4):407, 2019.

[32] Bashima Islam and Shahriar Nirjon. Zygarde: Time-sensitive on-device deep inference and adaptation on intermittently-powered systems. *arXiv preprint arXiv:1905.03854*, 2019.

[33] Vikram Iyer, Rajalakshmi Nandakumar, Anran Wang, Sawyer B Fuller, and Shyamnath Gollakota. Living iot: A flying wireless platform on live insects. In *The 25th Annual International Conference on Mobile Computing and Networking*, pages 1–15, 2019.

[34] Suraj Jog, Junfeng Guan, Sohrab Madani, Ruochen Lu, Songbin Gong, Deepak Vasisht, and Haitham Hassanieh. Enabling iot self-localization using ambient 5g signals. In *19th USENIX Symposium on Networked Systems Design and Implementation (NSDI 22)*, pages 1011–1026, 2022.

[35] Muzammil Jusoh, Tamer Aboufoul, Thennarasan Sabapathy, Akram Alomainy, and Muhammad Ramlee Kamarudin. Pattern-reconfigurable microstrip patch antenna with multidirectional beam for wimax application. *IEEE antennas and wireless propagation letters*, 13:860–863, 2014.

[36] Emrah Kaderli, İsrafil Bahçeci, Kathleen M Kaplan, and Bedri A Cetiner. On the use of reconfigurable antenna arrays for doa estimation of correlated signals. In *2016 IEEE Radar Conference (RadarConf)*, pages 1–5. IEEE, 2016.

[37] Sandeep Kamath and Joakim Lindh. Measuring bluetooth low energy power consumption. *Texas instruments application note AN092, Dallas*, 2010.

[38] Manikanta Kotaru, Kiran Joshi, Dinesh Bharadia, and Sachin Katti. Spotfi: Decimeter level localization using wifi. In *Proceedings of the 2015 ACM Conference on Special Interest Group on Data Communication*, pages 269–282, 2015.

[39] Swarun Kumar, Stephanie Gil, Dina Katabi, and Daniela Rus. Accurate indoor localization with zero start-up cost. In *Proceedings of the 20th annual international conference on Mobile computing and networking*, pages 483–494, 2014.

[40] Songfan Li, Hui Zheng, Chong Zhang, Yihang Song, Shen Yang, Minghua Chen, Li Lu, and Mo Li. Passive {DSSS}: Empowering the downlink communication for backscatter systems. In *19th USENIX Symposium on Networked Systems Design and Implementation (NSDI 22)*, pages 913–928, 2022.

[41] Riaz Ahmed Liyakath, Arash Takshi, and Gokhan Mumcu. Multilayer stretchable conductors on polymer substrates for conformal and reconfigurable antennas. *IEEE Antennas and Wireless Propagation Letters*, 12:603–606, 2013.

[42] Zhong-Liang Lu, Xue-Xia Yang, and Guan-Nan Tan. A multidirectional pattern-reconfigurable patch antenna with csrr on the ground. *IEEE Antennas and Wireless Propagation Letters*, 16:416–419, 2016.

[43] Yunfei Ma, Nicholas Selby, and Fadel Adib. Minding the billions: Ultra-wideband localization for deployed rfid tags. In *Proceedings of the 23rd annual international conference on mobile computing and networking*, pages 248–260, 2017.

[44] Angus CK Mak, Corbett R Rowell, Ross D Murch, and Chi-Lun Mak. Reconfigurable multiband antenna designs for wireless communication devices. *IEEE Transactions on Antennas and Propagation*, 55(7):1919–1928, 2007.

[45] Alex T Mariakakis, Souvik Sen, Jeongkeun Lee, and Kyu-Han Kim. Sail: Single access point-based indoor localization. In *Proceedings of the 12th annual international conference on Mobile systems, applications, and services*, pages 315–328, 2014.

[46] Mathworks. https://www.mathworks.com/help/antenna/ug/ray-tracing-for-wireless-communications.html, 2023.

[47] Matlab. https://www.mathworks.com/help/supportpkg/usrpradio/ug/qpsk-receiver-with-usrp-tm-hardware.html, 2022.

[48] Aidin Mehdipour, Tayeb A Denidni, Abdel-R Sebak, Christopher W Trueman, Iosif D Rosca, and Suong V Hoa. Mechanically reconfigurable antennas using an anisotropic carbon-fibre composite ground. *IET Microwaves, Antennas & Propagation*, 7(13):1055–1063, 2013.

[49] Ajith Kumar MM, Amalendu Patnaik, and Christos G Christodoulou. Design and testing of a multifrequency antenna with a reconfigurable feed. *IEEE Antennas and wireless propagation letters*, 13:730–733, 2014.

[50] Rajalakshmi Nandakumar, Vikram Iyer, and Shyamnath Gollakota. 3d localization for sub-centimeter sized devices. In *Proceedings of the 16th ACM Conference on Embedded Networked Sensor Systems*, pages 108–119, 2018.

[51] Naser Ojaroudi Parchin, Haleh Jahanbakhsh Basherlou, Yasir IA Al-Yasir, Ahmed M Abdulkhaleq, and Raed A Abd-Alhameed. Reconfigurable antennas: Switching techniques—a survey. *Electronics*, 9(2):336, 2020.

[52] Anuradha A Palsokar and SL Lahudkar. Frequency and pattern reconfigurable rectangular patch antenna using single pin diode. *AEU-International Journal of*

Electronics and Communications, 125:153370, 2020.

[53] Daniele Piazza, Prathaban Mookiah, Michele d'Amico, and Kapil R Dandekar. Experimental analysis of pattern and polarization reconfigurable circular patch antennas for mimo systems. *IEEE Transactions on Vehicular Technology*, 59(5):2352–2362, 2010.

[54] Qorvo. https://www.qorvo.com/products/p/RF5110G, 2022.

[55] Maurizio Rea, Aymen Fakhreddine, Domenico Giustiniano, and Vincent Lenders. Filtering noisy 802.11 time-of-flight ranging measurements from commoditized wifi radios. *IEEE/ACM Transactions on Networking*, 25(4):2514–2527, 2017.

[56] Daniel Rodrigo, Lluís Jofre, and Bedri A Cetiner. Circular beam-steering reconfigurable antenna with liquid metal parasitics. *IEEE transactions on antennas and propagation*, 60(4):1796–1802, 2012.

[57] Mohammad Rostami, Xingda Chen, Yuda Feng, Karthikeyan Sundaresan, and Deepak Ganesan. Mixiq: re-thinking ultra-low power receiver design for next-generation on-body applications. In *Proceedings of the 27th Annual International Conference on Mobile Computing and Networking*, pages 364–377, 2021.

[58] Nirupam Roy. Owlet: Insect-scale spatial sensing with 3d-printed acoustic structures. *GetMobile: Mobile Computing and Communications*, 25(2):14–20, 2021.

[59] Skyworks. https://store.skyworksinc.com/products/detail/sms7630006-skyworks/150612/, 2022.

[60] Elahe Soltanaghaei, Adwait Dongare, Akarsh Prabhakara, Swarun Kumar, Anthony Rowe, and Kamin Whitehouse. Tagfi: Locating ultra-low power wifi tags using unmodified wifi infrastructure. *Proceedings of the ACM on Interactive, Mobile, Wearable and Ubiquitous Technologies*, 5(1):1–29, 2021.

[61] Warren L Stutzman and Gary A Thiele. *Antenna theory and design*. John Wiley & Sons, 2012.

[62] Li Sun, Souvik Sen, Dimitrios Koutsonikolas, and Kyu-Han Kim. Widraw: Enabling hands-free drawing in the air on commodity wifi devices. In *Proceedings of the 21st Annual International Conference on Mobile Computing and Networking*, pages 77–89, 2015.

[63] Philip Taylor, Tara Crewe, Stuart Mackenzie, Denis Lepage, Yves Aubry, Zoe Crysler, George Finney, Charles Francis, Christopher Guglielmo, Diana Hamilton, et al. The motus wildlife tracking system: a collaborative research network to enhance the understanding of wildlife movement. *Avian Conservation and Ecology*, 12(1), 2017.

[64] Vida Vakilian, Hoang V Nguyen, Samer Abielmona, Sébastien Roy, and Jean-François Frigon. Experimental study of direction-of-arrival estimation using reconfigurable antennas. In *2014 IEEE 27th Canadian Conference on Electrical and Computer Engineering (CCECE)*, pages 1–4. IEEE, 2014.

[65] Arash Valizade, Mouhammad Ojaroudi, and Nasser Ojaroudi. Cpw-fed small slot antenna with reconfigurable circular polarizion and impdeance bandwidth characteristcis for dcs/wimax applications. *Progress In Electromagnetics Research C*, 56:65–72, 2015.

[66] Ambuj Varshney, Andreas Soleiman, and Thiemo Voigt. Tunnelscatter: Low power communication for sensor tags using tunnel diodes. In *The 25th Annual International Conference on Mobile Computing and Networking*, pages 1–17, 2019.

[67] Ambuj Varshney, Wenqing Yan, and Prabal Dutta. Judo: addressing the energy asymmetry of wireless embedded systems through tunnel diode based wireless transmitters. In *Proceedings of the 20th Annual International Conference on Mobile Systems, Applications and Services*, pages 273–286, 2022.

[68] Deepak Vasisht, Swarun Kumar, and Dina Katabi. {Decimeter-Level} localization with a single {WiFi} access point. In *13th USENIX Symposium on Networked Systems Design and Implementation (NSDI 16)*, pages 165–178, 2016.

[69] Jue Wang, Deepak Vasisht, and Dina Katabi. Rf-idraw: Virtual touch screen in the air using rf signals. *ACM SIGCOMM Computer Communication Review*, 44(4):235–246, 2014.

[70] Fan Wu and Kwai Man Luk. Wideband tri-polarization reconfigurable magneto-electric dipole antenna. *IEEE transactions on antennas and propagation*, 65(4):1633–1641, 2017.

[71] Yaxiong Xie, Jie Xiong, Mo Li, and Kyle Jamieson. md-track: Leveraging multi-dimensionality for passive indoor wi-fi tracking. In *The 25th Annual International Conference on Mobile Computing and Networking*, pages 1–16, 2019.

[72] Jie Xiong and Kyle Jamieson. {ArrayTrack}: A {Fine-Grained} indoor location system. In *10th USENIX Symposium on Networked Systems Design and Implementation (NSDI 13)*, pages 71–84, 2013.

[73] Jie Xiong, Karthikeyan Sundaresan, and Kyle Jamieson. Tonetrack: Leveraging frequency-agile radios for time-based indoor wireless localization. In *Proceedings of the 21st Annual International Conference on Mobile Computing and Networking*, pages 537–549, 2015.

[74] Xue-Song Yang, Bing-Zhong Wang, Sai Ho Yeung, Quan Xue, and Kim Fung Man. Circularly polarized reconfigurable crossed-yagi patch antenna. *IEEE Antennas and Propagation Magazine*, 53(5):65–80, 2011.

[75] Junbo Zhang, Elahe Soltanaghai, Artur Balanuta, Reese Grimsley, Swarun Kumar, and Anthony Rowe. {PLatter}: On the feasibility of building-scale power line backscatter. In *19th USENIX Symposium on Networked Systems Design and Implementation (NSDI 22)*, pages 897–911, 2022.

[76] Xiuyuan Zheng, Chen Wang, Yingying Chen, and Jie Yang. Accurate rogue access point localization leveraging fine-grained channel information. In *2014 IEEE conference on communications and network security*, pages 211–219. IEEE, 2014.

[77] Abdul Zohur, H Mopidevi, D Rodrigo, M Unlu, L Jofre, and Bedri A Cetiner. Rf mems reconfigurable two-band antenna. *IEEE Antennas and Wireless Propagation Letters*, 12:72–75, 2013.